A non-Gaussian probabilistic approach for estimating the equivalent static wind loads on structures from unsteady pressure field

Wafaa Kassir, Christian Soize, Jean-Vivien Heck, Fabrice de Oliveira

A NON-GAUSSIAN PROBABILISTIC APPROACH FOR ESTIMATING THE EQUIVALENT STATIC WIND LOADS ON STRUCTURES FROM UNSTEADY PRESSURE FIELD

Wafaa KASSIR[a,b], Christian SOIZE[a], Jean-Vivien HECK[b], and Fabrice DE OLIVEIRA[b]
[a]Université Paris-Est, Modélisation et Simulation Multi-Echelle, MSME UMR 8208 CNRS, 5 Bd Descartes, 77454 Marne-la-Vallée, France
[b]Centre Scientifique et Technique du Bâtiment (CSTB), 11 Rue Henri Picherit, 44300 Nantes, France
E-mail address: wafaa.kassir@cstb.fr

Abstract

A novel probabilistic approach is presented for estimating the equivalent static wind loads that produce a static response of the structure, which is "equivalent" in a probabilistic sense, to the dynamic responses due to the pressure random field induced by the wind. This approach has especially been developed for the case for which a large number of unsteady pressure measurements are carried out on complex structures (such stadium roofs) in a wind tunnel, the random pressure field is non-Gaussian, and the quasi-static part of the responses is important with respect to the dynamical part. The proposed approach is demonstrated with a simple illustrative example.
Keywords: *Equivalent static wind loads, Non-Gaussian pressure field, Probabilistic approach, Stochastic dynamics.*

INTRODUCTION

Some methodologies and numerical methods have been developed, which allow for computing the equivalent static wind loads, which induce the extreme values that are used for design [1–14]. In the case of structures with complex aerodynamic flows such as stadium roofs, for which the pressure field is non-Gaussian, and for which the dynamical response of the structure cannot be simply described by using only the first elastic modes (but require a good representation of the quasi-static responses), additional works must be carried out. It is assumed that the number of unsteady pressure sensors, which are required for performing experimental measurements of the unsteady pressure field applied to a structure with complex geometry, is relatively high (about $1{,}000$). Under this hypothesis, the number of time trajectories measured by the set of sensors over a sufficiently long duration T (about 10 minutes in scale 1) remains limited (about 100). Under these conditions, the measurements do not allow us to construct a statistically converged estimation of the extreme values of the dynamical responses, what are necessary for the determination of the equivalent static loads in order to reproduce the wind action on the structure taking into account the non-Gaussianity of the random pressure field. In this work, a new probabilistic approach is proposed to estimate the equivalent static forces of wind. Firstly, a generator of realizations of the non-Gaussian pressure random field is constructed by using the experiments, which allows for generating additional realizations to those measured in the wind tunnel. Secondly, the reduced-order dynamical model of the structure includes a quasi-static correction term that allows the convergence of the stochastic dynamical responses to be obtained by using only a small number of elastic modes.

Finally, the equivalent static forces are estimated by a maximum likelihood principle related to the random displacements of the structure, conditioned by the random observations that have to belong to a domain representing the extreme values of the observations (internal forces, displacement, etc.) in the structure. At the end of this paper, a simple application is presented in order to illustrate the proposed method. With respect to the existing methods, the novelties of the approach proposed, consist (1) in introducing quasi-static correction term for three dimensional structures that exhibit a numerous local modes interwined with global modes, in order to limit the number of modes in the construction of the reduced-order model, (2) in taking into account the non-Gaussianity of the pressure field for estimating the extreme values statistics of the responses, (3) in proposing an advanced non-Gaussian stochastic model of the pressure field based on its polynomial chaos expansion that is identified with measurements performed in a wind tunnel, in order to generate a large number of additional realizations that are required for estimating extreme values statistics of the responses, (4) in proposing a novel approach for estimating the static equivalent forces, based on the use of the maximum likelihood principal, without introducing classical envelopes that generally yield an increase of the equivalent static forces. The final objective of this work will be to analyze stadium structures subjected to wind loads for which unsteady pressure measurements are performed in wind tunnels.

STOCHASTIC MODELING, MODEL REDUCTION, AND STATIONARY STOCHASTIC RESPONSE

The stationary response of a weakly damped linear system subjected to external wind forces modeled by a stationary non-Gaussian stochastic process $\mathbb{P} = \{\mathbb{P}(t), t \in \mathbb{R}\}$ is analyzed. The frequency band of analysis is $\mathscr{B} = [0, \omega_c]$. The centered process of the pressure field $\mathbb{P}$ is written as $\mathbb{P}(t) = \underline{\mathbf{p}} + \mathbf{P}(t)$, where $\underline{\mathbf{p}}$ is the constant mean function of $\mathbb{P}$ and where $\mathbf{P}$ is a centered stationary non-Gaussian process. As the theoretical results on statistics on sample paths of Gaussian processes cannot be used, and as the stationary stochastic responses are not Gaussian, statistics on sample paths must be estimated using realizations of the stationary stochastic responses. For that, it is then necessary to construct a stochastic representation of $\mathbf{P}$, which is identified with the measurements, and to use this representation for generating additional realizations.

Computational model of the linear structural dynamics in the time domain

The structure is fixed (no rigid body displacement) and its computational linear dynamical model has m degrees of freedom (DOF). Let $\mathbf{Y}(t) = (Y_1(t), \ldots, Y_m(t))$ be the displacement vector (translations and/or rotations) and let $\mathbf{F}(t) = (F_1(t), \ldots, F_m(t))$ be the vector of external wind forces (forces and/or bending moments) applied to the structure, which is written as $\mathbf{F}(t) = [A_c]\,\mathbb{P}(t)$ in which $[A_c]$ is the $(m \times m_{\text{exp}})$ controllability matrix and where $\mathbb{P}(t) = (\mathbb{P}_1(t), \ldots, \mathbb{P}_{m_{\text{exp}}}(t))$ is the vector that corresponds to the wind tunnel pressure measurements in m_{exp} points of the structure (see for instance [15, 16]). An observation $\mathbb{U}(t) = (\mathbb{U}_1(t), \ldots, \mathbb{U}_{m_u}(t))$ in the structure can be displacements, internal forces, stresses or strains. For a given duration T and a given domain $\mathscr{D}$ of values of $\mathbb{U}$, the equivalent static forces (associated with $\mathbb{U}$, T, and $\mathscr{D}$) are constructed in order to maximize the probability that $\mathbb{U}(T)$ belongs to $\mathscr{D}$. The observation is written as $\mathbb{U}(t) = [A_o]\,\mathbf{Y}(t)$ in which $[A_o]$ is the observation matrix. Let $\mathbb{U}_{\max}$ (or $\mathbb{U}_{\min}$) be the maximum (or the minimum) of $\mathbb{U}(t)$ on $[0, T]$, where $[0, T]$ is the time window for the signal processing. For several observations, these equivalent static forces are merged in order to construct a set of algebraically independent equivalent static forces.

Reduced-order model in time domain

The non usual modal analysis including a quasi-static term [17] is used for constructing a reduced-order model considering N elastic modes (the quasi-static term is added in order to accelerate the convergence

with respect to N). The response $\mathbf{Y}(t)$ can be written as $\mathbf{Y}(t) = \underline{\mathbf{y}} + \mathbf{X}(t)$, where the static response $\underline{\mathbf{y}}$ is such that $[K]\,\underline{\mathbf{y}} = \underline{\mathbf{f}}$ with $\underline{\mathbf{f}} = [A_c]\,\underline{\mathbf{p}}$, and where $[K]$ is the $(m \times m)$ stiffness matrix. The displacement vector $\mathbf{X}(t) = (X_1(t), \ldots, X_m(t))$ is the non-Gaussian stationary centered process that is written, for all t, as

$$\mathbf{X}(t) = [\mathscr{S}_N^c]\,\mathbf{P}(t) + [\varphi_N]\,\mathbf{Q}(t)\,, \tag{1}$$

$$\ddot{\mathbf{Q}}(t) + [D_N]\,\dot{\mathbf{Q}}(t) + [\lambda_N]\,\mathbf{Q}(t) = \boldsymbol{\mathscr{P}}_N^c(t)\,, \tag{2}$$

in which $\boldsymbol{\mathscr{P}}_N^c(t) = [\phi_N^c]\,\mathbf{P}(t)$, and where $\mathbf{Q}(t) = (Q_1(t), \ldots, Q_N(t))$ is a non-Gaussian stationary centered process verifying Eq. (2) for all t, $[\varphi_N]$ is the $(m \times N)$ matrix of the elastic modes, $[\lambda_N]$ is the $(N \times N)$ diagonal matrix of the square of the eigenfrequencies, $[D_N]_{\alpha\beta} = 2\xi_\alpha\omega_\alpha\delta_{\alpha\beta}$ is the $(N \times N)$ generalized damping matrix depending on the damping rates ξ_α, $[\phi_N^c] = [\varphi_N]^T\,[A_c]$, and the $(m \times m_{\text{exp}})$ matrix $[\mathscr{S}_N^c]$ represents the quasi-static terms. Using Eqs. (1) and (2), observation $\mathbb{U}(t)$ can be written as

$$\mathbb{U}(t) = \underline{\mathbf{u}} + \mathbf{U}(t) \quad \text{with} \quad \mathbf{U}(t) = [\mathscr{U}_N^{oc}]\,\mathbf{P}(t) + [\phi_N^o]\,\mathbf{Q}(t)\,, \tag{3}$$

in which $[\mathscr{U}_N^{oc}] = [A_o][\mathscr{S}_N^c]$, $[\phi_N^o] = [A_o]\,[\varphi_N]$, and $\underline{\mathbf{u}} = [A_o]\,\underline{\mathbf{y}}$. At time t, the equivalent force $\mathbb{F}^e(t) = (\mathbb{F}_1^e(t), \ldots, \mathbb{F}_m^e(t))$, which is defined by $\mathbb{F}^e(t) = [K]\,\mathbf{Y}(t)$, is written as

$$\mathbb{F}^e(t) = \underline{\mathbf{f}} + \mathbf{F}^e(t) \quad \text{with} \quad \mathbf{F}^e(t) = [K]\,\mathbf{X}(t)\,. \tag{4}$$

Substituting $\mathbf{X}(t)$ by its approximation defined by Eqs. (1) and (2) yields,

$$\mathbf{F}^e(t) = [\mathscr{F}_N^c]\,\mathbf{P}(t) + [\mathcal{F}_N^{\mathbf{Q}}]\mathbf{Q}(t)\,, \tag{5}$$

in which $[\mathcal{F}_N^{\mathbf{Q}}] = [K]\,[\varphi_N]$ and where $[\mathscr{F}_N^c] = [K]\,[\mathscr{S}_N^c]$. The time response $\mathbf{Q}(t)$ for $t \in [0, T]$, is computed at the sampling points $t_1, \ldots, t_{n_p}$ by using its discrete Fourier transform $\widehat{\mathbf{Q}}(\omega_q) = [\widehat{h}_N(\omega_q)]\widehat{\boldsymbol{\mathscr{P}}}_N^c(\omega_q)$, in which $q = 1, \ldots, n_p$, and where $\omega_1, \ldots, \omega_{n_p}$ are the corresponding sampling frequencies, and $[\widehat{h}_N(\omega)]_{\alpha\beta}$ $= \delta_{\alpha\beta}(-\omega^2 + 2i\omega\xi_\alpha\omega_\alpha + \omega_\alpha^2)^{-1}$. For $q = 1, \ldots, n_p$, $\widehat{\boldsymbol{\mathscr{P}}}_N^c(\omega_q)$ is computed by using the Fast Fourier Transform, and for $k = 1, \ldots, n_p$, $\mathbf{Q}(t_k)$ is deduced by the Inverse Fast Fourier Transform. The values of $\mathbf{Q}(T) = \mathbf{Q}(n_p)$ can then be deduced.

GENERATOR OF REALIZATIONS OF THE NON-GAUSSIAN PROCESS P

It is assumed that n_r independent realizations of the vector-valued stochastic process $\mathbf{P}$ have been measures in the wind tunnel. Generally, this number n_r of realizations is not sufficient to estimate the extreme values statistics that will be used to compute the equivalent static forces. It is then necessary to generate additional realizations of the pressure field from the n_r measurements. The generator is obtained by constructing a polynomial chaos representation of process $\mathbf{P}$, which is identified using the experimental measurements. The methodology consists in performing a Karhunen-Loeve (KL) statistical reduction [18, 19] of the non-Gaussian process $\mathbf{P}$ and then in identifying a representation of the random vector constituted by the coordinates of such a KL reduction by a finite polynomial chaos expansion [20]. The coefficients of the polynomial chaos expansion are estimated from the experimental measurements using the maximum likelihood principle [21–23]. This optimization problem is solved either by using a random search algorithm or by using a deterministic optimization such as the "interior points" method [24].

ESTIMATION OF THE EQUIVALENT STATIC FORCES

Taking into account Eq. (4), the equivalent static force $\mathbb{f}^{e,s} = (\mathbb{f}_1^{e,s}, \ldots, \mathbb{f}_m^{e,s})$ associated with observation $\mathbb{U}(t)$ defined by Eq. (3), is written as $\mathbb{f}^{e,s} = \underline{\mathbf{f}} + \mathbf{f}^{e,s}$. For $t = T$, Eq. (5) is written as,

$$\mathbf{F}^e(T) = [\mathscr{F}_N^c]\,\mathbf{P}(T) + [\mathcal{F}_N^{\mathbf{Q}}]\mathbf{Q}(T)\,. \tag{6}$$

As the dimension m_{exp} of the random vector $\mathbf{P}(T)$ is much larger (for instance 700 to 1,000) than the dimension of $\mathbf{Q}(T)$ and $\mathbf{U}(T)$, a Principal Component Analysis (PCA) of the random vector $\mathbf{P}(T)$ is introduced in order to reduce the dimension and to normalize the random quantities,

$$\mathbf{P}(T) \simeq \underline{\mathbf{p}}_T + \sum_{j=1}^{N_{\text{PCA}}} \sqrt{\Lambda_j}\, H_j\, \mathbf{a}^j\,, \tag{7}$$

in which N_{PCA} is the reduction order such that $N_{\text{PCA}} \leq m_{\text{exp}}$, $\underline{\mathbf{p}}_T$ is the empirical mean of $\mathbf{P}(T)$, $(\mathbf{a}^1, \ldots, \mathbf{a}^{N_{\text{PCA}}})$ are the eigenvectors associated with the N_{PCA} largest eigenvalues $\Lambda_1 \geq \Lambda_2 \geq \ldots \geq \Lambda_{N_{\text{PCA}}}$ of the covariance matrix $[C_{\mathbf{P}(T)}]$ of $\mathbf{P}(T)$, and $\mathbf{H} = (H_1, \ldots, H_{N_{\text{PCA}}})$ is the random coordinates of the PCA. The equivalent static force $\mathbf{f}^{e,s}$ can then be computed by

$$\mathbf{f}^{e,s} = [\mathscr{F}_N^c]\,\mathbf{p}^{\text{MV}} + [\mathcal{F}_N^{\mathbf{Q}}]\,\mathbf{q}^{\text{MV}} \quad \text{with} \quad \mathbf{p}^{\text{MV}} \simeq \underline{\mathbf{p}}_T + \sum_{j=1}^{N_{\text{PCA}}} \sqrt{\Lambda_j}\,\eta_j^{\text{MV}}\,\mathbf{a}^j\,, \tag{8}$$

in which the vectors $\boldsymbol{\eta}^{\text{MV}} = (\eta_1^{\text{MV}}, \ldots, \eta_{N_{\text{PCA}}}^{\text{MV}})$ and $\mathbf{q}^{\text{MV}} = (q_1^{\text{MV}}, \ldots, q_N^{\text{MV}})$ are such that

$$(\boldsymbol{\eta}^{\text{MV}}, \mathbf{q}^{\text{MV}}) = \arg\{\max_{(\boldsymbol{\eta},\mathbf{q})} \int_{\mathscr{D}^c} p_{\mathbf{H},\mathbf{Q}(T),\mathbf{U}(T)}(\boldsymbol{\eta}, \mathbf{q}, \mathbf{u})\, d\mathbf{u}\}\,, \tag{9}$$

where $p_{\mathbf{H},\mathbf{Q}(T),\mathbf{U}(T)}(\boldsymbol{\eta}, \mathbf{q}, \mathbf{u})$ is the joint probability density function of random vectors $\mathbf{H}$, $\mathbf{Q}(T)$, $\mathbf{U}(T)$, and where $\mathscr{D}^c$ is the centered domain associated with $\mathbf{U}$, which is such that Proba$\{\mathbb{U}(T) \in \mathscr{D}\}$ = Proba$\{\mathbf{U}(T) \in \mathscr{D}^c\}$. It is assumed that $\mathscr{D}^c$ can be written as $\mathscr{D}^c = \Pi_{j=1}^{m_u} \mathscr{D}_j^c$ with $\mathscr{D}_j^c = (\mathscr{D}_{\text{inf},j}^c, \mathscr{D}_{\text{sup},j}^c)$. The bounds $\mathscr{D}_{\text{inf},j}^c$ and $\mathscr{D}_{\text{sup},j}^c$ are defined with respect to the sign of the mean observation $\underline{u}_j$, for $j = 1, \ldots, m_u$, as follows

$$\begin{array}{lllll} \text{si} & \underline{u}_j \geq 0 & , & \mathscr{D}_{\text{inf},j}^c = \underline{U}_{\max,j} & , \quad \mathscr{D}_{\text{sup},j}^c = \alpha \underline{U}_{\max,j}\,, \\ \text{si} & \underline{u}_j < 0 & , & \mathscr{D}_{\text{inf},j}^c = \alpha \underline{U}_{\min,j} & , \quad \mathscr{D}_{\text{sup},j}^c = \underline{U}_{\min,j}\,, \end{array} \tag{10}$$

where $\underline{U}_{\max,j}$ (resp. $\underline{U}_{\min,j}$) is the mean value of the maximum (resp. the minimum) of U_j on $[0, T]$, and where α is a positive constant (for instance $\alpha = 1000$). In Eq. (9), the non-Gaussian probability density function is estimated using the Gaussian kernel method of the non-parametric statistics [25, 26] and the integration over set $\mathscr{D}^c$ is explicitly (algebraically) calculated. The optimization problem defined by Eq. (9), which is non-convex, is solved using the "active set" algorithm without constraints [27].

APPLICATION

The application considered is a model of the Maine-Montparnasse Tower in Paris, for which measurements have been carried out [28, 29]. The aim of this application is to present a validation of the proposed theory on a simple structure. The origin o of the orthonormal reference frame $oxyz$ is located at the base (the foundation level) of the Tower, the x-axis is perpendicular to the largest faces of the Tower while the y-axis is perpendicular to the smallest ones, and the z-axis is vertical (see Fig. 1). We are interested in the bending of the Tower in the plane xoz. The computational model [29] is made up of

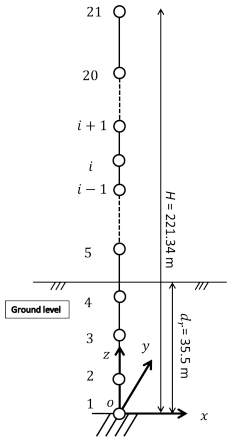

FIGURE 1 - Finite element model of the Maine-Montparnasse Tower .

a linear Timoshenko-beam finite element model with variable inertia. This 2D beam is discretized into 20 Timoshenko-beam finite elements. There are 21 nodes over the whole structure, with 3 degrees of freedom by node (63 DOFs over the whole structure): x-displacement, z-displacement, and y-rotation (rotation around oy). At node 1 (the foundation level that is the base), the DOFs x and z are locked, and the flexibility of the foundations is accounted for by an elastic connection following y-rotation. The following quantities have experimentally been measured [28, 29]: the total static flexibility at the node 21 along x-axis is 0.267×10^{-7} m/N; the first bending eigenfrequency in the xoz plane is 0.20 Hz and the second one is 0.92 Hz; the damping rate of the first bending mode is 0.0083. The finite element model as been updated using these measured quantities and yields the experimental measures for the total static deflection and the first two bending modes. The reduced-order model is constructed with the quasi-static term and with the first two bending elastic modes ($N = 2$). The damping rates for the two first modes are chosen as 0.0083. This application is used for experimentally validating the method and also for carrying out a sensitivity analysis with respect to the non-Gaussianity of the pressure field. Consequently, three models of the pressure field are constructed and correspond to a local transformation of the Gaussian longitudinal fluctuations, noted V, of the wind velocity. Since the experimental measurements of the pressure field are not available, the pressure field is generated as a transformation of V whose realizations are numerically simulated. The Harris power spectral density function [30] and the extended Davenport model [31–33] for the cross-spectral density function of V are used in a Gaussian random field model for which the realizations are constructed by using [34, 35].

- Model 1. This model does not correspond to the experiments. The pressure field is a linear function of V. Consequently, the pressure field is Gaussian.

- Model 2. This model corresponds to the experiments for which the measured reference wind velocity is $\underline{V}_R = 17$ m/s. For the experimental validation, the pressure field is generated by using a quadratic function of V. Consequently, the pressure field is non-Gaussian. It should be noted that the non-Gaussianity rate is relatively small for the considered value of $\underline{V}_R$.

- Model 3. Again, this model does not correspond to the experiments. The pressure field is constructed as a nonlinear empirical function of V, specially introduced to analyze the non-Gaussian effects.

Experimental validation using model 2

Let $\mathbb{U}_d^1(t) = Y_{62}(t) - Y_3(t) \times H$ be the relative x-displacement of node 21 (top of the Tower) in the relative frame attached to the base (the raft) that is in y-rotation. The displacement $Y_{62}(t)$ is the absolute

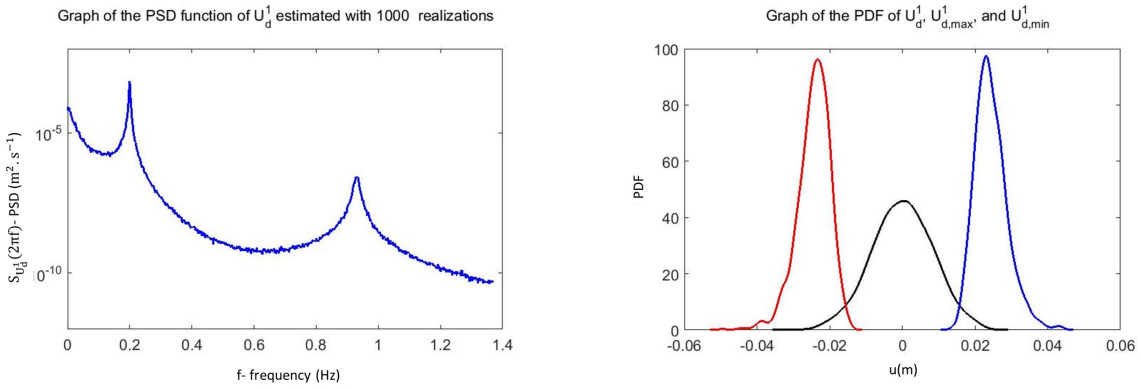

FIGURE 2 - Graph $f \mapsto S_{U_d^1}(2\pi f)$ of observation process U_d^1 (left fig.). Graph $u \mapsto p_{U_d^1}(u)$ of U_d^1 (black line, central curve), $u \mapsto p_{U_{d,\max}^1}(u)$ of $U_{d,\max}^1$ (blue line, right curve), and $u \mapsto p_{U_{d,\min}^1}(u)$ of $U_{d,\min}^1$ (red line, left curve)(right fig.).

x-displacement of node 21 in the reference frame and $Y_3(t)$ is the rotation of the raft around oy at node 1. The height of the Tower is $H = 221.34$ m. The observation $\mathbb{U}_d^1(t)$ is written as $\mathbb{U}_d^1(t) = \underline{u}_d^1 + U_d^1(t)$ in which $m_u = 1$ and where $\underline{u}_d^1$ is the mean value. Model 2 is used for generating the pressure field from the velocity field V. The mean of the extreme values of $\mathbb{U}_d^1(t)$ has been measured (see [28, 29]) and is used for the experimental validation. The method presented before is used to generate 1,000 independent realizations of $\{\mathbf{P}(t), t \in [0\,, T]\}$ with $T = 748$ s. Fig. 2 (left) shows the power spectral density function $f \mapsto S_{U_d^1}(2\pi f)$ of the centered observation $U_d^1(t)$. This figure shows that there is a non negligible quasi-static contribution in the band $[0\,, 0.12]$ Hz. For this observation, the mean value $\underline{u}_d^1$ is positive, then the worst case of the observation is the maximum case. For the experimental comparison, the numerical values gives $\underline{\mathbb{U}}_{d,\max}^1/\underline{u}_d^1 = (4.64 \times 10^{-2})/(2.20 \times 10^{-2}) = 2.11$, which matches with the experimental value given in [28, 29] and which allows us to validate the proposed approach for the presented application. It should be noted that the corresponding gust loading factor is $g_d^{+,1} = 2.93$ while the use of a Gaussian approximation would yield $g_{d,\text{gauss}}^1 = 3.27$. Fig. 2 (right) shows the probability density functions of the random variables U_d^1, $U_{d,\max}^1 = \max_{t\in[0,T]} U_d^1(t)$, and $U_{d,\min}^1 = \min_{t\in[0,T]} U_d^1(t)$. It can be seen that these are not symmetric (non-Gaussianity of the pressure field).

Validation of the method for computing the equivalent static forces and convergence analysis with respect to the number of realizations

In this section, Model 2 is used. Let $\mathbb{U}^1$ and $\mathbb{U}^2$ be the shear force and the bending moment in the beam section at node 1, and $\mathbb{U}^3$ and $\mathbb{U}^4$ be the shear force and the bending moment in the beam section at node 13. For $i = 1, 2, 3, 4$, we write $\mathbb{U}^i = \underline{u}^i + U^i$ in which $\underline{u}^i$ is the mean value. It should be noted that, for $\mathbb{U}^1$ and $\mathbb{U}^2$, the mean values of the shear force and the bending moment (induced by the mean value of the pressure field) are maximum, and for $\mathbb{U}^4$, the bending moment associated with the second elastic mode is maximal and $\mathbb{U}^3$ is the associated shear force.

Illustration of the equivalent static forces computation. Let $\mathbb{f}^{2,e,s}$ be the equivalent static force computed for the observation $\mathbb{U}^2$. The components of the equivalent static forces along z-axis are zeros. For 1,000 realizations, Fig. 3 shows the equivalent force along x-axis and the moment around y-axis. It should be noted that the moment at node 1 (see Fig. 3 (right)) corresponds to the reaction of the elastic connection for the rotation around oy. Note also that the exterior moments are zeros for the other DOFs. Fig. 3 (left) shows that the amplitude of the component x of the equivalent forces at node 21 is smaller than the amplitude at node 20. This is due to the fact the wind effects surface associated with the node 21 has an area smaller than the area associated with the node 20.

Validation of the method for computing the equivalent static forces. To validate the approach pro-

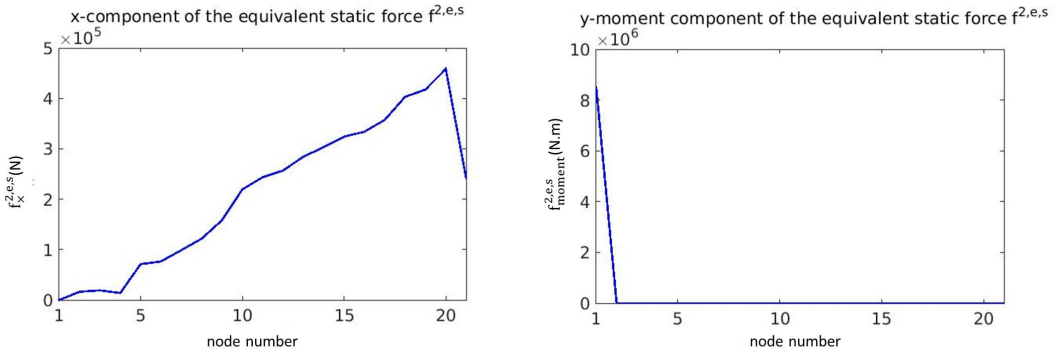

FIGURE 3 - Graph of the x-component of $\mathbb{f}^{2,e,s}$ (left figure) and graph of the y-moment component of $\mathbb{f}^{2,e,s}$ (right figure).

TABLE 1 - Numerical values of the variables related to $\mathbb{u}^{2,e,s}$ and $\mathbb{u}^{4,e,s}$.

	$\underline{u}^i$	$\underline{\mathbb{U}}^i_{\min}$	$\mathbb{u}^{i,e,s}$	$\mathscr{D}^i_{\sup}$
$\mathbb{U}^2$(N.m)	-3.15×10^8	-6.52×10^8	-6.52×10^8	-6.52×10^8
$\mathbb{U}^4$(N.m)	-7.39×10^7	-1.62×10^8	-1.62×10^8	-1.62×10^8

posed to compute the equivalent static forces, the equivalent static observation $\mathbf{u}^{e,s}$ (calculated in the previous paragraph) is recomputed with the static problem $\mathbf{u}^{e,s} = [A_o]\,\mathbf{x}^{e,s}$ in which $\mathbf{x}^{e,s}$ is the equivalent static displacement such that $[K]\,\mathbf{x}^{e,s} = \mathbf{f}^{e,s}$. For $i = 2$ and $i = 4$, let $\mathbb{u}^{i,e,s} = \underline{u}^i + u^{i,e,s}$ be the equivalent static observation corresponding to $\mathbb{U}^i$. The numerical values corresponding to $\mathbb{U}^2$ and $\mathbb{U}^4$ are given in Table 1. The mean values $\underline{u}^2$ and $\underline{u}^4$ are negative, then the worst case of the observation will be the minimum case. The value of $\mathbb{u}^{i,e,s}$ is equal to $\underline{\mathbb{U}}^i_{\min}$ for $i = 2$ and $i = 4$ and consequently, the computation of the equivalent static forces is validated for the hypotheses chosen. Note that the optimizer finds the mean $\underline{\mathbb{U}}^i_{\min}$ as an optimal value because the input upper bound is $\mathscr{D}^i_{\sup} = \underline{\mathbb{U}}^i_{\min}$ and the probability density function for which the maximum likelihood is searched, presents its maximum for a value slightly higher than $\mathscr{D}^i_{\sup}$, because of the dissymmetry of the non-Gaussian probability density function.

Analysis of the convergence with respect to the number of realizations. To analyze the convergence as a function of the number ν of realizations, four cases are studied, for which 100 "experimental" realizations ($n_r = 100$) are used with $\nu = 1000, 10000, 100000$. Fig. 4 shows the probability density functions of U^2, $U^2_{\max}$, and $U^2_{\min}$ for these four cases. These figures show that the convergence is reached for about 1,000 realizations, which matches with the results obtained from the convergence analysis of the extreme values. This means that the probability density functions of the extreme values can correctly be estimated with 1,000 realizations.

Analysis of the non-Gaussianity and the convergence with respect to the realizations number

The analysis of the non-Gaussianity is made using 1,000 realizations. For the three models of the pressure field defined before, Table 2 presents the gust loading factors g_{gauss} computed with the usual Gaussian formula [36], and g^+ and g^- computed with the realizations of the observations without introducing any hypotheses or approximations. The analysis of the results given in this table shows that, even though model 1 be Gaussian, the values of g_{gauss} are different from the values of $g^+ \simeq g^-$. This difference comes from the fact that the usual Gaussian formula is obtained by using a Poisonian hypothesis of the crossing time series for the maximum values. In our case, such a usual Gaussian formula seems to give an overestimation with respect to the statistical estimation directly constructed from the realizations. These differences also remain for models 2 and 3 in spite of the fact that the latter are non-Gaussian.

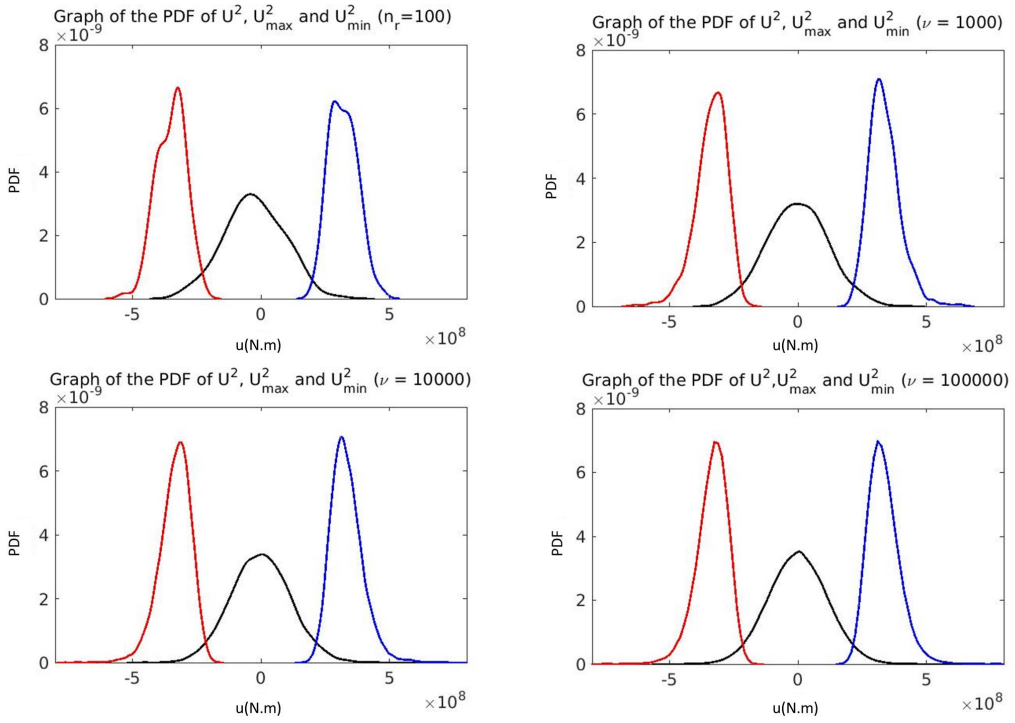

FIGURE 4 - Graphs of the probability density function of U^2 (black line, central curve), $U^2_{\max}$ (blue line, right curve) and $U^2_{\min}$ (red line, left curve) for $n_r = 100$ (upper left), $\nu = 1000$ (upper right), $\nu = 10000$ (lower left) and $\nu = 100000$ (lower right).

TABLE 2 - The gust loading factors.

	Model 1		Model 2			Model 3		
	g_{gauss}	$g^+ \simeq g^-$	g_{gauss}	g^+	g^-	g_{gauss}	g^+	g^-
$\mathbb{U}^1$	3.20	2.928	3.320	2.871	2.876	3.391	2.953	3.080
$\mathbb{U}^2$	3.264	2.941	3.265	2.883	2.887	3.283	2.617	2.672
$\mathbb{U}^3$	3.273	2.961	3.274	2.952	2.950	3.001	2.732	2.763
$\mathbb{U}^4$	3.316	3.034	3.316	3.017	3.006	3.389	2.809	2.841

CONCLUSION

In this paper, a generator of realizations of the non-Gaussian random pressure field is constructed on the base of a polynomial chaos expansion for which the coefficients are estimated by using a set of available realizations (coming from measurements in a wind tunnel). This generator allows the non-Gaussian property of the unsteady pressure field to be reproduced and a large number of independent realizations to be generated in order to be able to estimate the probability density functions of the extreme values of the structural responses. A in time-domain reduced-order model with the quasi-static acceleration term is constructed, which allows us to accelerate the convergence of the structural responses with respect to the retained small number of the elastic modes of the structure. Finally, a new probabilistic method is proposed for the computation of the equivalent static forces induced by the quasi-static and dynamical effects of the wind on structures, preserving the non-Gaussian property and without introducing the concept of response envelopes. An application to a simple structure has been made in order to validate the proposed methodology and an application to a complex structure such a stadium roof is in progress.

REFERENCES

[1] Blaise N, Canor T, Denoël V, 2016. Reconstruction of the envelope of non-Gaussian structural responses with principal static wind loads . *J. Wind Eng. Ind. Aerodyn.*, 149:59 – 76.

[2] Chen X, Kareem A, 2004. Equivalent static wind loads on buildings : New model. *J. Struct. Eng.*, 130(10):1425–1435.

[3] Chen X, Zhou N, 2007. Equivalent static wind loads on low-rise buildings based on full-scale pressure measurements. *Eng. Struct.*, 29(10):2563–2575.

[4] Gu M, Hunag Y, 2015. Equivalent static wind loads for stability design of large span roof structures. *Wind Struct.*, 20(1):95–115.

[5] Holmes JD, 2002. Effective static load distributions in wind engineering. *J. Wind Eng. Ind. Aerodyn.*, 90(2):91–109.

[6] Kasperski M, Niemann HJ, 1992. The L.R.C (load-response-correlation)-Method. A General Method of Estimating Unfavourable Wind Load. Distributions for Linear and Non-linear Structural Behaviour. *J. Wind Eng. Ind. Aerodyn.*, 43(1-3):1753–1763.

[7] Katsumara A, Tamura Y, Nakamura O, 2007. Universal wind load distribution simultaneously reproducing largest load effects in all subject members on large-span cantilevered roof. *J. Wind Eng. Ind. Aerodyn.*, 95(9):1145–1165.

[8] Kumar KS, Stathopoulos T, 2000. Wind loads on low building roofs: A stochastic perspective. *J. Struct. Eng.*, 126(8):944–956.

[9] Liang S, Zou L, Wang D, Huang G, 2014. Analysis of three dimensional equivalent static wind loads of symmetric high-rise buildings based on wind tunnel tests. *Wind Struct.*, 19(5):565–583.

[10] Lou W, Zhang L, Huang MF, Li QS, 2015. Multiobjective equivalent static wind loads on complex tall buildings using non-gaussian peak factors. *J. Struct. Eng.*, 141(11).

[11] Repetto MP, Solari G, 2004. Equivalent static wind actions on vertical structures. *J. Wind Eng. Ind. Aerodyn.*, 92(5):335–357.

[12] Sun W, Gu M, Zhou X, 2015. Universal equivalent static wind loads of fluctuating wind loads on large-span roofs based on POD compensation. *Adv. Struct. Eng.*, 18(9):1443–1459.

[13] Yang QS, Chen B, Wu Y, Tamura Y, 2013. Wind-Induced Response and Equivalent Static Wind Load of Long-Span Roof Structures by Combined Ritz-Proper Orthogonal Decomposition Method. *J. Struct. Eng.*, 139(6):997–1008.

[14] Zhou X, Gu M, 2010. An approximation method for computing the dynamic responses and equivalent static wind loads of large-span roof structures. *Int. J. Struct. Stab. Dy.*, 10(5):1141–1165.

[15] Vinet J, De Oliveira F, 2011. Etudes aérodynamiques de dimensionnement au vent du Stade Vélodrome de Marseille : nouvelles configurations. Technical Report EN-CAPE 11.114 C V2, CSTB, Nantes, France.

[16] Vinet J, De Oliveira F, Barre C, Fayette E, Consigny F, Vondiere R, 2015. Wind effects on stadium refurbishment the example of Stade Velodrome in Marseille, France. In *Proceedings of the 14th International Conference on Wind Engineering (ICWE14)*, pages 1–10, Porter Alegre, Brazil.

[17] Ohayon R, Soize C, 1998. *Structural Acoustic and Vibration*. Academic Press, San Diego, London.

[18] Karhunen K, 1947. Uber lineare methoden in der wahrscheinlichkeitsrechnung. *American Academy of Science, Fennicade Series A, I*, 37:3–79.

[19] Loève M, 1948. Fonctions aléatoires du second ordre, supplément à P. Levy. In *Processus Stochastique et Mouvement Brownien*, Paris. Gauthier Villars.

[20] Ghanem R, Spanos PD, 1991. *Stochastic Finite Elements: a Spectral Approach*. Springer-Verlag, New York. See also the revised edition (2003), Dover Publications, New York.

[21] Desceliers C, Ghanem R, Soize C, 2006. Maximum likelihood estimation of stochastic chaos representations from experimental data. *Int. J. Numer. Meth. Eng.*, 66(6):978–1001.

[22] Perrin G, Soize C, Duhamel D, Funfschilling C, 2012. Identification of polynomial chaos representations in high dimension from a set of realizations. *SIAM J. Sci. Comput.*, 34(6):A2917–A2945.

[23] Soize C, 2017. *Uncertainty quantification. An Accelerated Course with Advanced Applications in Computational Engineering*. Springer, New York.

[24] Byrd RH, Hribar ME, Nocedal J, 1999. An interior point algorithm for large-scale nonlinear programming. *SIAM J. Optimiz.*, 9(4):877–900.

[25] Givens GH, Hoeting JA, 2013. *Computational Statistics*. Wiley, New York, second edition.

[26] Horova I, Kolacek J, Zelinka J, 2012. *Kernel Smoothing in Matlab*. World Scientific, Singapor.

[27] Gill PE, Murray W, Wright MH, 1981. *Pratical Optimization*. Academic Press, London.

[28] CEBTP (Center for Research and Studies for Buildings and Public Works),15 June 1978. Effets du vent sur la Tour Maine-Montparnasse. Technical report. Comlpementary report 1st October 1978.

[29] Krée P, Soize C, 1986. *Mathematics of Random Phenomena*. Reidel, New York. French version: Mécanique Aléatoire, Dunod, Paris, 1983.

[30] Harris RI, 1970. The nature of the wind. In Institution Of Civil Engineers, editor, *Seminar in the Modern Design of Wind-Sensitive Structures*, Construction Industry Research and Information Association, pages 29–55, London, England.

[31] Davenport AG, 1961. The application of statistical concepts of the wind loading of structures. *Proceeding of the Institution of Civil Engineers*, 19(4):449–472.

[32] Biétry J, Simiu E, Sacré C, 1978. Mean wind profiles and charge of terrain roughness. *J. Struct. Div.*, 104(10):1585–1593, October.

[33] Simiu E, Scanlan RH, 1996. *Wind Effects on Structures. Fundamentals and Applications to Design*. John Wiley & Sons, New York, third edition.

[34] Shinozuka M, 1971. Simulation of Multivariate and Multidimensional Random Processes. *J. Acoust. Soc. Am.*, 49(1B):357–368.

[35] Poirion F, Soize C, 1995. Numerical methods and mathematical aspects for simulation of homogeneous and non homogeneous Gaussian vector fields. In P. Krée and W. Wedig, editors, *Probabilistic Methods in Applied Physics*, pages 17–53. Springer-Verlag, Berlin.

[36] Davenport AG, 1967. Gust loading factors. *J. Struct. Div.*, 93(3):11–34.